Available online at www.sciencedirect.com
ScienceDirect
EPSL
Earth and Planetary Science Letters 253 (2007) 485–496
www.elsevier.com/locate/epsl

Rare destructive earthquakes in Europe: The 1904 Bulgaria event case

Bertrand Meyer [a,*], Michel Sébrier [a], Dimitar Dimitrov [b]

[a] Laboratoire de Tectonique, UMR CNRS 7072, Université Paris 6, Case 129, Tour 46-0, 2[E], 4 pl. Jussieu, 75252 Paris Cedex 05, France
[b] Institute of Geodesy, Bulgarian Academy of Sciences, Sofia, Bulgaria

Received 3 April 2006; received in revised form 11 October 2006; accepted 6 November 2006
Available online 6 December 2006
Editor: C.P. Jaupart

Abstract

Seismic hazard is difficult to assess in regions of low strain rates. A major limitation often relates to the absence of large instrumentally recorded events precluding any comparison between seismological data and paleoseismic or morphotectonic informations. We take advantage of the 1904 M_s~7.1 earthquake that struck the southern edge of stable Eurasia and investigate if morphotectonic and paleoseismic observations can provide a reliable estimate of the seismic potential of slow-slipping faults. We have conducted a paleoseismic study of the Krupnik normal fault thought to be responsible for the event. A section of the fault bearing remnants of a 2 m-high scarp has been selected at the base of triangular facets. The trenching site locates where the scarp cuts across colluviums washed from the bedrock facetted slopes. We excavated two neighbouring trenches, one across a well-preserved portion of the scarp, and one across a portion degraded by a landslide. The excavations reveal a set of coarse colluvial units faulted against bedrock and affected by secondary fissures. Faulting appears to have resulted from a single event with normal throw greater than 1.3 m that occurred before the emplacement of the landslide. Accelerator Mass Spectrometry (AMS) radiocarbon dates of charcoal samples are consistent with the interpretation that the Krupnik Fault slipped recently, most probably in 1904, after a long lasting (>10 ka) period of quiescence. The morphotectonic and paleoseismic observations yield seismic moment estimates compatible with the instrumental magnitude of the event and indicate that destructive and infrequent earthquakes typify the regional seismic behaviour.

Keywords: active tectonics; Bulgaria; morphology; paleoseismology; seismic hazard

1. Introduction

Assessing seismic hazard in regions of low strain rates is difficult because the seismogenic sources are often poorly known. The moderate levels of seismicity that characterise such regions reveal short of illuminating active faults. The slip-rates are small, a few tenths of mm/yr at most, and the active faults appear uneasy to differentiate from older structures because of their limited topographic imprint. These regions can nevertheless host rare but destructive earthquakes (e.g., Basel [1], Bhuj [2]) or earthquake clusters (e.g., New Madrid [3,4]) challenging the study of faults with small slip-rates and very long recurrence intervals. A major limitation is that most destructive historical earthquakes are often too old to allow a comparison between instrumental data and macroseismic, paleosismic, or morphotectonic information. The large earthquake that struck Bulgaria in 4 April 1904 by the southern edge of stable Eurasia offers such a

* Corresponding author.
E-mail address: bertrand.meyer@lgs.jussieu.fr (B. Meyer).

0012-821X/$ - see front matter © 2006 Elsevier B.V. All rights reserved.
doi:10.1016/j.epsl.2006.11.011

possibility and we have investigated the fault thought to be the source for this destructive event. The event, known as the Struma earthquake from the many towns and villages devastated in the neighbourhood of the Struma River, had long remained a puzzling event [5,6]. Considered as the largest shallow earthquake ever recorded in Europe with magnitude estimates up to $M_S = 7.8$, neither the surface break nor the source fault were known. The situation has cleared up recently with a re-evaluation of the instrumental and macroseismic data [7] and a morphotectonic investigation conducted in the epicentral area [8]. Both studies demonstrated that the early magnitudes reported were largely overestimated and concluded to a significant downsizing of the event. Indeed, the reappraisal of the instrumental and macroseismic data concluded to M_s magnitude estimates of 7.1–7.2, values compatible with the limited size of active faults encountered in the epicentral region. Remnants of a 2 m-high scarp were discovered along the Krupnik Fault, a 20 km long normal fault that locates entirely inside the area of maximum intensity (Fig. 1). Considering the absence of similarly recent scarps on the neighbouring faults, Meyer et al. [8] concluded that the Krupnik Fault most probably hosted the 1904 earthquake, a scenario recently tested with Coulomb stress interactions studies [9].

We have conducted paleoseismic investigations to examine the former hypothesis, start to decipher the seismic history of the Krupnik Fault, and estimate the repeat time of 1904 type events. First, we summarize the tectonic setting of the area and the overall morphology of the Krupnik Fault by combining SPOT Satellite imagery

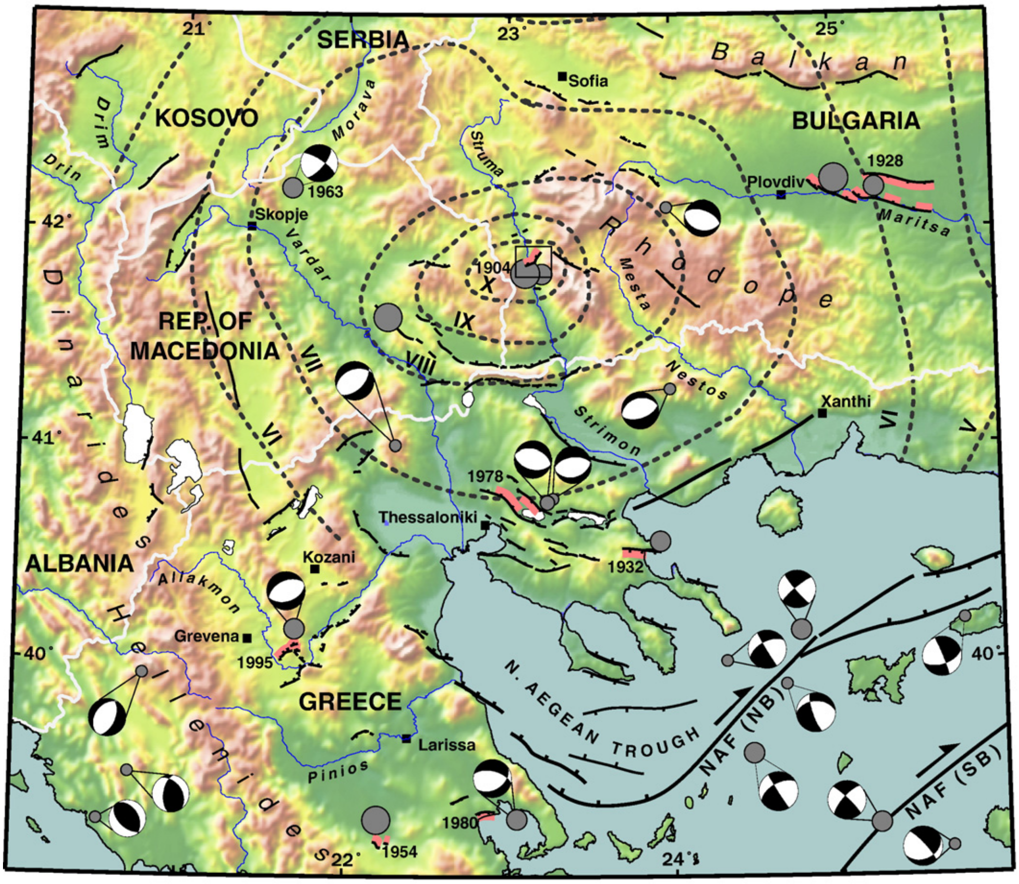

Fig. 1. Seismotectonic map of the region struck by the 4 April 1904 Struma earthquake. Foreshock and main shock locations are from Ref. [5], isoseismals (dotted grey lines, MSK intensity scale) from Ref. [6]. Regional active faults compiled from bathymetry (offshore), geological studies and satellite imagery (onshore). NB and SB respectively for North and South branches of the North Anatolian Fault. Faults associated with earthquake breaks are outlined in red. USGS seismicity is indicated; large symbols are events with M_s magnitude equal to or larger than 7, intermediate with $6 \le M_s < 7$, and small with $5 \le M_s < 6$. Fault plane solutions are from Harvard CMT catalogue. Box outlines the area enlarged in Fig. 2.

with SRTM topographic data. Then, detailed topographic profiles of the trench site are used to analyse the small-scale morphology of the recent scarp. Trenching across the scarp is applied to retrieve the Late Quaternary fault evolution and ^{14}C dated charcoals are used to place bounds on the age of the scarp and landscape evolution. Finally, we discuss our results in relation with the assessment of seismic hazard in regions of low-rates of deformation.

2. Tectonic setting of the Krupnik Fault

Bulgaria and Northern Greece locate north of the Aegean in a region experiencing crustal extension and thought to be the northernmost part of the Aegean stretched domain (e.g., [10]; Fig. 1). The stretching is accounted by a set of normal faults cutting across the compressive structures of the Alpine belt. The faults strike WNW to EW in Northern Greece and in the Republic of Macedonia and cut at right angles across the fabric of the Dinarides and Hellenides belts. The faults strike mostly EW to ESE in Bulgaria where they are slightly oblique to the structural trends in the Rhodope and the Balkan belts. The overall fault network and the well-constrained focal solutions available point towards a NS directed regional extension (Fig. 1). The faults are distributed throughout the region. They are segmented and bound a series of small horsts and grabens, a few tens of kilometres long at most, that are much smaller than the large systems of central Greece and western Turkey, west and east of the Aegean Sea. Accordingly, the deformation rates in Northern Greece and Bulgaria are much smaller than within the Aegean and appear to decrease northward. GPS measurements indicate 2–3 mm/yr of NS extension across Bulgaria and northern Greece [11–13] of which at most 1 mm/yr is absorbed in Bulgaria [14,15]. The Krupnik Fault is one of the faults that contributes the modest extension in Bulgaria.

The Krupnik Fault locates halfway between Sofia and Thessaloniki. The fault strikes NE–SW, is about 20 km long and exposed on both sides of the Struma River (Fig. 2). The fault separates footwall basement rocks to the south from a Neogene hangingwall basin to the north. The basin is an asymmetric half-graben that has been progressively filled by a 1-km thick sedimentary sequence tilted against the fault. The tectonic evolution of the basin has been relatively simple and can be summarized as follows [8]. Normal faulting initiated in Sarmatian times about 12.5 Ma ago and isolated a fluviolacustrine basin. Hangingwall subsidence and progressive infilling of the basin took place during Meotian and Dacian times meanwhile coeval footwall uplift prevented significant accumulation of sediments south of the fault. Only the youngest units found in the hangingwall are represented in the footwall. Infilling of the basin ended about 4 Ma ago when the regional environment shifted from depositional to erosionnal conditions. Since then, there has been a significant lowering of the base level and the Struma River and its tributaries have incised the basin. Quaternary alluvial stepped-terraces made of coarse to medium-sized conglomerates were emplaced during the post Dacian dissection of the basin. The uppermost terrace levels cap the Neogene beds more than 200 m above the Struma River. Morphologic evidence attests to continuing fault activity since the onset of the incision of the basin (Fig. 2c). The fault bounds a NW facing 300–400 m-high mountain front made of triangular facets. The Pontian–Dacian sediments that cap the shoulders of the facets have the same attitude but a much higher elevation than the Pontian–Dacian sediments in the footwall (Fig. 2b). The base of the Pontian is cut by the fault at an elevation of about 450 m in the hangingwall and found at about 1050 m heights in the footwall. This provides a long-term throw-rate of about 0.1 mm/yr in the past 5.8 Myr. Assuming the rate remained uniform since the inception of faulting, the 1.3 km basement step would have accumulated over the last 13 Ma, in agreement with the Sarmatian age of the oldest sediments in the basin. Taking an average fault dip close to 45° yields a slip-rate of 0.15 mm/yr.

Faulted Quaternary is found northeast of the Struma River where the fault morphology is the most impressive and the basin the less dissected. There, remnants of Neogene sediments capped by thin Quaternary terrace levels are preserved along the base of triangular facets incised by tributaries of the Struma River (Fig. 3a,b). Natural sections of the fault plane have been exhumed along the tributaries. The fault dips 60° to the NW in all sections and Quaternary conglomerates are sliced within the fault zone in several ones (Fig. 3c). The evidence for the most recent fault reactivation occurs as a 2 m-high scarp running for about 4 km long across gullies and intervening ridges at the base of the facets. The length and the shape of the scarp led Meyer et al. [8] to conclude it resulted from the last seismic slip on the Krupnik Fault. The freshness of the scarp and its location with respect to the epicentral area of the 1904 earthquake led them to infer it corresponds to remnants of the 1904 surface break. Assuming a uniform long-term throw-rate of 0.1 mm/yr, the 2 m-high scarp would account for the occurrence of a single earthquake in the last 20 ka. The next section further investigates the late Holocene history of the Krupnik Fault and discusses the

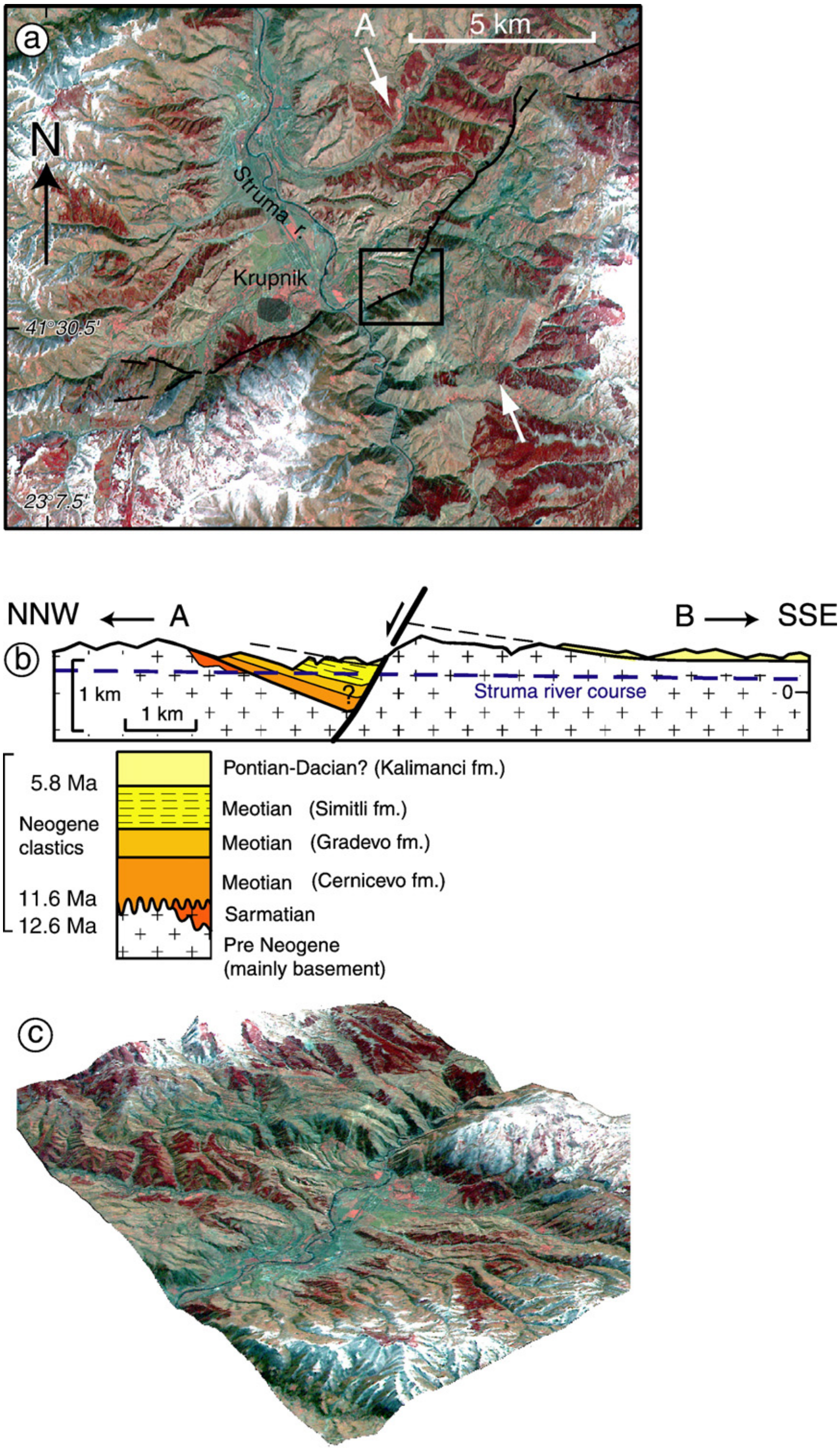

Fig. 2. The Krupnik half-graben. a, Fault trace superimposed on a SPOT4 color composition (20 m pixel-size). The fault runs at the base of a NW facing cumulative scarp and separates hangingwall Neogene sediments to the North from a footwall basement high to the South. Box outlines the area shown in Fig. 3a. b, Geologic section simplified from Ref. [8], see location on a. c, 3-D perspective view towards the Krupnik Fault obtained by draping the SPOT image over the SRTM-3s digital elevation model. The Struma River flows southward within a narrow canyon incised in the footwall block.

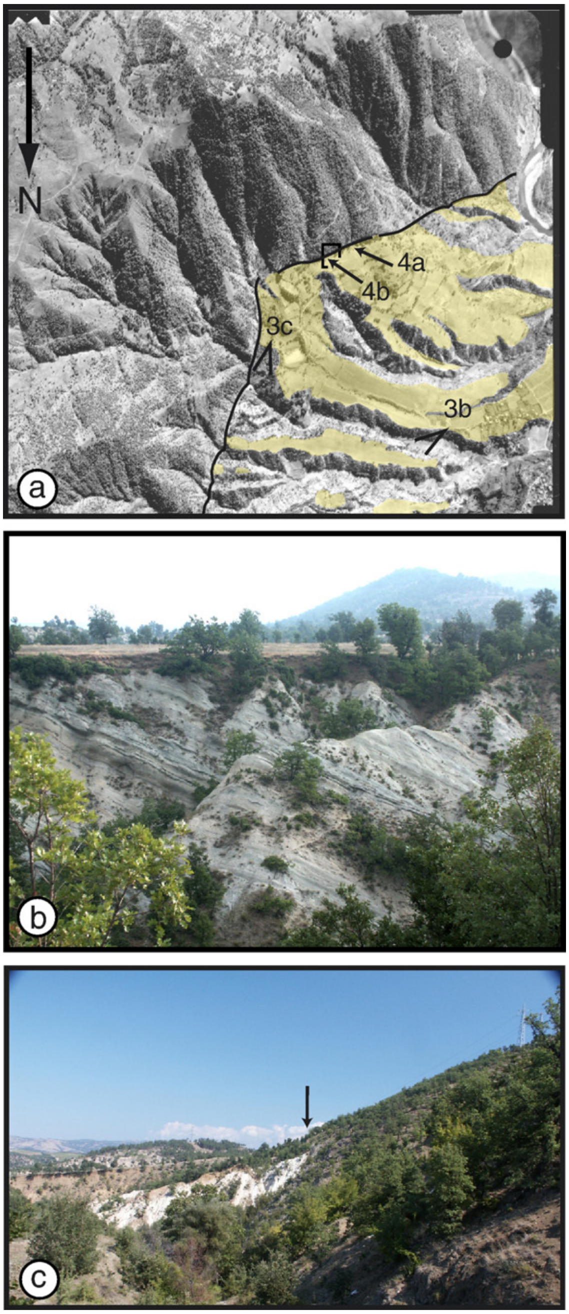

Fig. 3. Geomorphology of the Krupnik Fault. a, Enlargement of aerial photograph. The cumulative fault scarp is made of a series of triangular facets. The flat-topped basement (top right) is hanging 400 m above the sedimentary basin (lower left) capped by Quaternary terrace remnants (yellow patches). Location and orientation of pictures 3b,c are indicated. Numbered arrows refer to field photographs of the slope break in Fig. 4. Box indicates location of the paleoseismic site described in Fig. 5. b, Southeast dipping alternations of sandstones and siltstones (Upper Neogene Simitli Formation) overlain by a thin Quaternary terrace. c, Fault (black arrow) separating sediments of the Simitli formation (left) from granitic and gneissic basement (right).

results of the paleoseismic excavations performed across the scarp.

3. Paleoseismic investigations

3.1. The trench site

Except for the Struma River, the drainage network crossing the Krupnik Fault flows northward, towards the hangingwall. Nowhere else can be found a stream flowing towards the footwall, precluding the possibility to find places with fine sediments ponded against the scarp. In addition, the erosionnal environment prevailing in the whole area does not favour the preservation of detailed paleoseismologic records. Accounting for all these limitations, we selected a portion of the fault close to the sharp fault bend about 1.5 km NE of the of Struma River (Fig. 3). NE of the bend, the Quaternary terraces that mantle the Neogene sediments have been dissected by numerous tributaries of the Struma River. SW of the bend, the terraces have been less dissected than to the north and much less than anywhere else in the basin. Large outcrops of the uppermost terraces abut against the base of a triangular facet where they have been covered by colluviums. Locally, the colluviums merge with small debris fans emplaced at the outlet of scarce hill-slope restricted gullies. The gullies are dry and incised in the debris fans whose surfaces covered by a recent soil suggest aggradation is no longer efficient. Erosion has been limited preventing exhumation of the fault plane and allowing for the conservation of subtle topographic features. The faulted morphology is well-preserved and the recent scarp can be followed over more than a kilometre distance. At few places, the scarp is pristine, cut into basement, and steeply dipping (>70°) to the North (Fig. 4a). At most places, the scarp is cut into colluviums washed out from the facetted slopes and accumulating downslope over the terraces (Fig. 4b). The colluviums scarp is typically 2–5 m wide and less steep (<40°) than the bedrock free face. The colluviums scarp is slightly degraded; remnants of a retreating free face are still distinguishable at few places and small landslides have occurred at several places (Fig. 5a). We selected the trench site along a 40 m long section of the colluviums scarp with a high potential for the preservation of recent deposits. The site locates between the western edge of a small alluvial fan and the eastern edge of a landslide. We used a high precision theodolithe–distancemetre to level eight, 50–70 m long topographic profiles perpendicular to the scarp. For such a survey, the uncertainties on profile point positions are only due to the roughness of the topographic surface.

Fig. 4. Field observations of the Krupnik Fault scarp at the base of the facetted slope, see 3a for location. a, View to SSW of steep basement scarp separating brecciated basement (left) from coarse fanglomerate (right). The step is about 1.8 m-high and marks a bedrock free face. b, View to SSW of degraded scarp in colluvial material. Vertical arrows highlight the slope offset and indicate the location of trench 1. Horizontal arrow outlines the toe of a landslide along the base of the scarp and indicates location of trench 2.

The uncertainties are less than a centimetre on the smooth topography of the colluviums-covered terraces down scarp. They reach up to 5 cm for the more rugged parts of the scarp and the colluviums-mantled slopes up scarp. Overall, the measured profiles look similar and show well-constrained slopes on either side of the scarp (Fig. 5b). The profiles have greater slopes up scarp (30°) on the facetted morphology than down scarp (4°) on the terraced morphology. The height of the scarp is comparable from one to another profile and the average vertical offset of the slopes is 1.5 m. Two profiles, P4 and P5, display a subtle down warping of the lower slope and a tenuous topographic depression at the scarp base. Three other profiles, P6–8 measured across the portion of the scarp degraded by a landslide, also share distinctive features. They display a much wider slope break than profiles P1–5. The slope break is 12–18 m wide and extends from the front to the scar of the landslide. The landslide lies at the base of the scarp and appears as a small topographic bulge, about 5 m long and 50 cm-high on the profiles. The comparison between profiles P7 and P5 indicates that the collapsed material has been removed from the upper part of the scarp and emplaced over the lower part of the scarp. We excavated two neighbouring trenches, T1 across the scarp of profile P5, and T2 across the degraded scarp of profile P7, by the edge of the landslide. Both locations favoured the preservation of recent deposits at the scarp base, the latter also providing a sedimentary unit subsequent to the formation of the scarp, hence to the earthquake. The stratigraphy of the trenches and the mapping of the walls are described in the next section.

3.2. The excavations

The trenches are almost 10 m long, 1 m wide, 2–3 m deep, and have been dug on a N150° orientation (Fig. 6). They are less than 20 m apart and expose Holocene to modern deposits, mostly colluviums, over a gneissic substratum. Both trenches provide convincing observations for recent normal faulting with disrupted units and fissures testifying for a recent surface break.

3.2.1. Trench T1

The trench T1 has a maximum depth of 2.45 m and displays two main parts. A 6 m long, southern portion excavated across the slope of the scarp and a 4 m long, northern portion across the flat area downscarp. The southern portion of the trench displays recent colluviums over a sharp, 43° NE dipping contact with basement. The basement-colluviums contact (F, Fig. 6a,b) has been reactivated by distributed gravitational collapse and

Fig. 5. The excavation site. a, The schematic map provides the location of trenches and the position of topographic profiles. Black dots locate the measured points. Quaternary terraces and colluviums (yellow) lie at the base of the scarp (light grey) and are locally covered by a recent landslide (dark grey). b, The profiles (red curves) highlight a 1.5 m-high slope offset across the scarp. Crosses are measured points and dashed strait lines approximate the surface slope far from the scarp. Simplified logs of trench 1 and 2 are projected respectively along profiles P4 and P7. c, Comparison between profile P5 (dashed blue curve) and neighbouring profile P7 cutting across middle of the landslide (red curve). The shaded areas figure out negative (blue) and positive (orange) topographic changes with respect to profile P5.

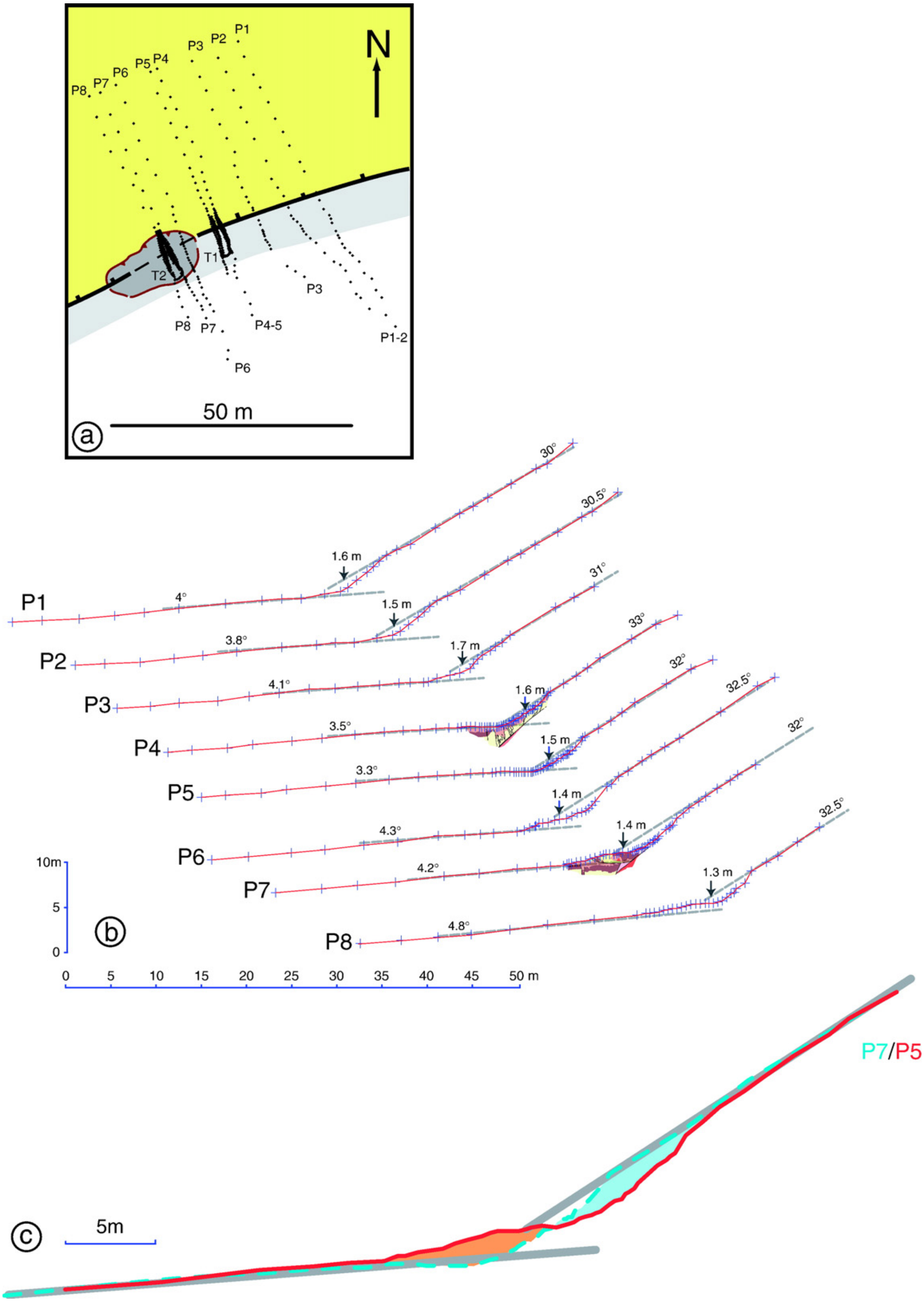

N
P1
P2
P3
P4
P5
P6
P7
P8
T1
T2
P4-5
P1-2
50 m
a
30°
30.5°
31°
33°
32°
32.5°
1.6 m
1.5 m
1.7 m
1.4 m
1.3 m
4°
3.8°
4.1°
3.5°
3.3°
4.3°
4.2°
4.8°
10m
5
0
0
5
10
15
20
25
30
35
40
45
50 m
b
P7/P5
5m
c

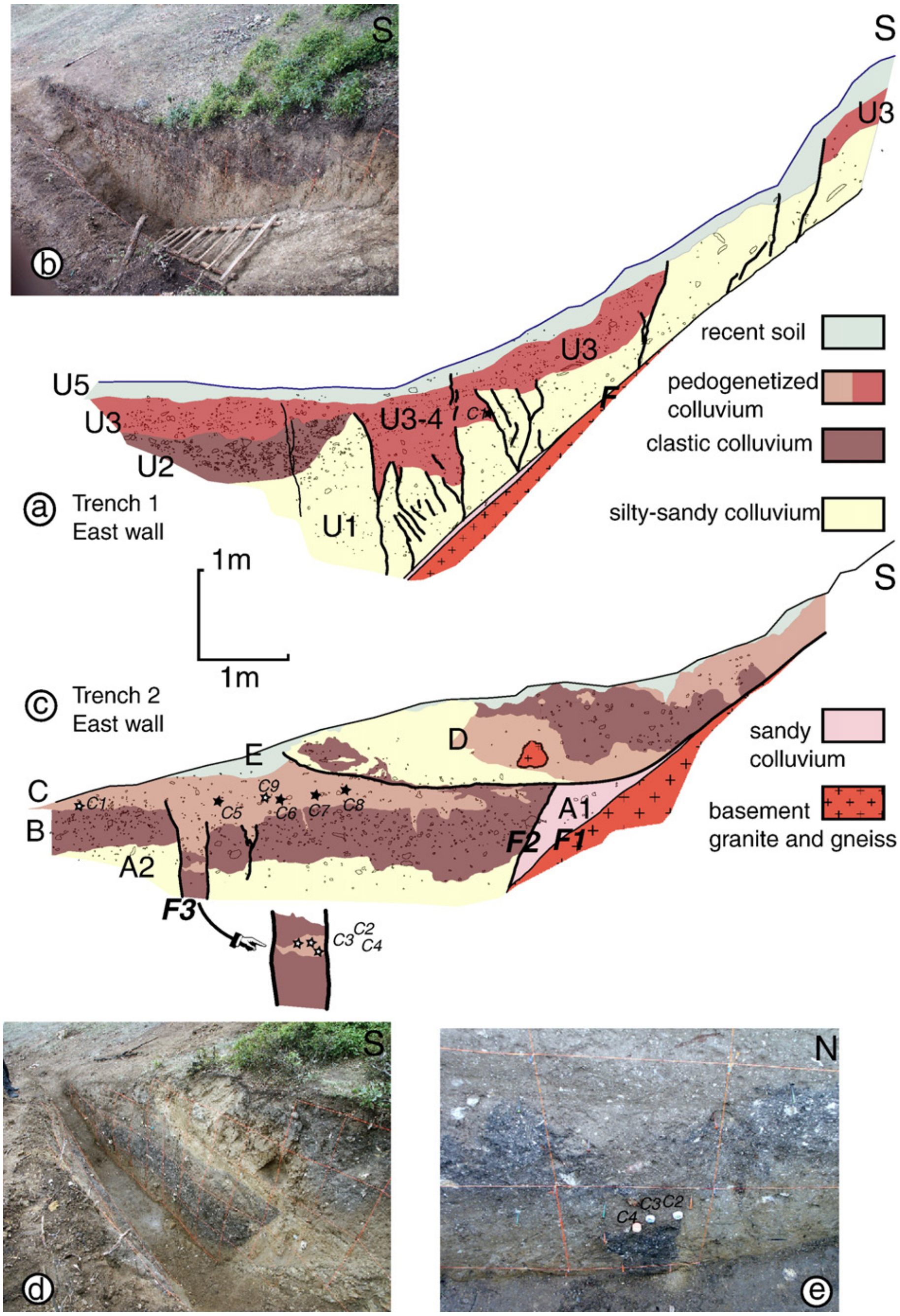

Fig. 6. The walls of the trenches. The stratigraphy consists of coarse colluviums overlain by a recent soil (see Section 3.2 for detailed descriptions). Colours outline the stratigraphic content of the labelled units and the possible correlation between the units of each trench. Numbered stars indicate the position of dated charcoals (see Table 1). Black stars locate samples collected on the eastern wall, white stars refer to samples collected on the western wall (not shown) and projected on the eastern wall. a, Eastern wall of trench 1. Numerous faults and fissures disrupt the colluviums. Upslope, the faults and fissures merge with colluviums-basement contact. b, Overall photograph of trench 1 showing the contact between the brown and light grey colluviums. c, Eastern wall of trench 2. A landslide cuts across main fault F2 and sharp contact F1 between colluviums and basement. A secondary fissure, enlarged below for location of charcoals, disrupts the colluviums. d, Overall photograph of the eastern wall. Warping of the clast-rich colluviums (black unit) against main fault is clear. Toe of landslide, resting above colluviums and crosscutting the main fault, is distinguishable. e, Photograph of secondary fault F3 and fissure in the downthrown block (western wall). Pieces of clast-rich (black unit) colluviums B are mixed with pieces of pedogenetized (light beige unit) colluviums C that contained numerous charcoal wood fragments. Circular marks locate the position of samples C2, C3, C4.

normal fault motion. The northern portion of the trench is made of flat lying colluvial and alluvial deposits, which have accumulated on the downthrown block.

Five units can be distinguished from base to top in the hangingwall: U1, colluvial deposits; U2, gravely alluvial deposits; U3, pedogenetized material mainly of colluvial origin; U4, reworked colluviums and soil; U5, present-day soil. U1 corresponds to a yellowish, clayish–silty sand that contains some isolated substratum clasts. Its matrix appears slightly weathered but the clasts are well-preserved. The unit, which is thinner upslope where it lies over the basement than downslope where it has accumulated in the hangingwall, typifies colluviums. U2 unit, a light brown, sandy and pebbly deposit, is only found in the northern part of the trench. It is made of well-preserved clasts and pebbles within a slightly weathered clayish silty matrix. U2 displays a debris flow facies typical of fanglomerates. The contact between U1 and U2 appears relatively progressive so that emplacement of both units is mostly coeval. U2 corresponds to the distal edge deposits of an alluvial fan well developed further East and represents the alluvial deposits contemporary with the colluvial unit U1. Both units are slightly weathered and their aggradation appears no longer active. These units probably emplaced during a period of efficient erosion that planed the facetted slopes. U3 is a dark brown to dark grey pedogenetic horizon that developed either from U1 or U2. It is well exposed within the southern part of the trench and corresponds to the B-horizon of a soil that emplaced on U1 colluviums. U3 is also present atop the alluvial unit U2 in the northernmost trench exposures. U4 is a dark to pale grey unit made of a clayish, silty–sandy colluvial deposits with isolated clasts. U4 is often difficult to distinguish from U3 since it is made of reworked pieces of U3, already a pedogenetized colluviums, mixed with soil fragments. It is seen atop U3 mostly at the base of the scarp. U5 is a greyish, organic rich, horizon corresponding to the present-day soil.

The stratigraphic relationships between the units, simple at both trench tips, are more complicated in between. U3 is not observed in the middle of the southern part of the trench, and U5 lies directly over U2. Conversely, U4 locates by the slope break where it overthickens U3. In fact, emplacement of U4 corresponds to a fissure infill in which material of U3 has been reworked from above and mixed with pieces of soil. U4 has almost completely filled the fissure whose location is denoted by a small topographic depression still visible at the scarp base on profiles P4 and P5. Detailed logging of the trench walls allowed mapping series of fissures within all the units described. The many fissures seen upslope are branching off the basement-colluviums contact and the most important ones show generally a normal fault displacement. Overall, the fissures network indicates that the upslope colluviums slid down on the major contact in response to fissure opening at the scarp base. Most of the fissures disrupt the oldest units (U1–4), and very few the youngest, U5. Off the few fissures disrupting the base of U5, all locate within the slope, none along the flat area downscarp. This suggests that gravitational collapse of the colluviums occurs along the scarp slope. Given the coarse stratigraphy of the units, the fissures disrupting U1–U4 appear to result from a single, sudden faulting event. This event postdates U3 and predates most of U5 since the few fissures affecting U5 result from subsequent gravitational sliding. It is not possible to ascertain that U4, whose transition with the upper part of U3 is difficult to pinpoint, postdates the event. That the topmost part of U4 contains reworked pieces of U3 removed from upslope and that U4 fills the upper part of an open fissure at the scarp base suggests it is the case.

3.2.2. Trench T2

The trench T2 locates parallel to and 15 m West of T1, and has a maximum depth of 2.55 m. There is a sharp contact (F1 on Fig. 6c) between basement and colluviums. As for T1, the contact has favoured sliding and collapse. It is nonetheless easier to distinguish tectonic motion from gravitational effects since only the upper part of the contact coincides with the toe of a well-expressed landslide. F1 isolates two very different geologic formations: the substratum made of weathered metamorphic rocks that form the bulk of the Krupnik Fault footwall and recent to modern superficial formations overlying the hangingwall sediments. Six superficial formations can be distinguished from base to top: A1, sandy colluvial deposits; A2, silty–sandy colluvial deposits; B, pedogenetized colluvial deposits; C, colluviated soil; D, slid colluviums and soil lenses; and E, present-day soil. A1 is a yellowish, clayish, coarse sandy colluvial deposits that contains some isolated basement clasts. It is restricted to the southern bottom of the trench and has a triangular shape that results from non-stratigraphic contacts. The upper part of A1 is truncated by a landslide while its edges are in normal fault contact both with the footwall basement rocks and with the colluviums that form most of the hangingwall block. A2 is a brown, clayish, silty–sandy colluvial deposits that contains some isolated basement clasts. Notwithstanding its brown colour that seems to result from a subsequent episode of pedogenesis, A2 appears fairly similar to A1. Both units might be coeval, A1 being a little more sandy, hence more proximal, than A2. B is a dark grey, organic rich, silty and gravely colluvial deposits. Its transition with A2 appears progressive while its upper limit with C is sharp and more pronounced. B may be interpreted as the topmost part of a soil that developed after aggradation of the colluviated material found in A2 and B and before the emplacement of the subsequent colluviums. C is a pale grey, clayish and gravely colluvial deposits that rests on B. The colluviums have been pedogenetized making it difficult to distinguish the unit C from the present-day soil E, except where they are separated by a landslide. *D* is a landslide made of the previous units (A to C units) that appear mixed and disorganized. E corresponds to the light greyish present-day soil and exhibits variable thicknesses.

The stratigraphic relationships between the units are clear and simpler than in the previous trench. The deformation is less distributed than in trench 1 and the units are disrupted by a few well-localized faults. Three normal faults and a large fissure with sharp edges can be observed in the bottom of the trench. F1, the 40°N dipping contact between basement and colluviums, is cross-cut by a steep normal fault F2. F2 dips 63° due North, a value similar to that of the Krupnik Fault where observed in section (Fig. 3c) and similar to that of pristine basement scarp where preserved (Fig. 4a). F2 separates the squeezed colluviums A1 from the flat colluviums A2-B–C. The latter are disrupted by a 30 cm wide fissure emplaced on a small antithetic fault F3 whose upward tip vanishes within unit C. Finally, the landslide D emplaced over all the colluviums and truncates F1 and F2. The structural relationships between the units are suggestive, as for trench 1, of a single sudden event postdating C and predating D. Indeed, the fissure infill involves a large fragment of unit C intercalated between pieces of unit B. The fissure resulted from a sudden break disrupting units A2-B–C as shown by the offset of the flat lying boundary between units A2 and B across fault F3. Units A1–A2-B are warped and faulted against fault F2. The offset required to restore the contact between B and A2 to the level of colluviums A1 is about 90 cm. This value provides a lower bound on the fault throw since the upper part of A1 is truncated by the landslide and erosive. Accounting for the offset across F3 by adding several tens centimetres more provides a total normal throw in excess of 1.3 m. This is in good agreement with the average scarp height measured across the offset slope. Altogether, the detailed morphology and the trenching evidences substantiate that the scarp has resulted from a single and recent normal faulting event. The next section discusses the age of the event as well as the Late Quaternary evolution of the landscape in light of ^{14}C radiometric dating from detrital charcoals collected in the trenches.

3.3. ^{14}C dating and late Pleistocene fault evolution

We collected ten charcoal samples; one at the base of unit U3 in trench 1, and 9 within unit C in trench 2. For unit C, six samples are distributed within a middle-unit level and three others are grouped within a large fragment of the unit found in the large fissure F3 at the bottom of the trench (Fig. 6c). Although most of the samples originated from the same unit, we aimed to date them all with ^{14}C radiometric AMS analyses. Sample T2-C3 was small and has unfortunately been destroyed during dating processing but the other samples have been successfully dated (Table 1). The samples from unit C yielded seven modern ages and one belonging to the 13th A.D. Century. Each modern sample provided three to five possible calibrated time intervals of which the most likely falls within the 19th century for all but one sample. Accounting for the largest possible values, the modern samples belong to A. D. 1667–1953 while the older sample falls within A.D. 1218–1264. Considering the age clustering and the spatial distribution of the samples, the colluviums unit C probably emplaced during modern times and incorporated

Table 1
Radiocarbon dates

Sample	$\delta^{13}C$ (‰)	Radiocarbon Age (BP)	Unit	Calibrated age (1σ)
T1-C1*	−27.0	11080±90	U3	B.C. 11126–10973
T2-C1	−22.6	80±35	C	A.D. 1696–1726; A.D. 1814–1836; A.D. 1844–1851; **A.D. 1877–1917**
T2-C2*	−26.7	112±36	C	A.D. 1691–1729; **A.D. 1810–1891**; A.D. 1908–1924
T2-C3				
T2-C4*	−25.5	104±33	C	A.D. 1694–1727; **A.D. 1812–1893**; A.D. 1906–1918
T2-C5*	−19.25	160±45	C	A.D. 1667 –1695; **A.D. 1726–1783**; A.D. 1796–1813; A.D. 1853–1868; A.D. 1908–1953
T2-C6	−24.7	125±35	C	A.D. 1683 –1709; A.D. 1717–1735; A.D. 1805–1828; **A.D. 1831–1890**; A.D. 1910–1930
T2-C7	−25.2	120±35	C	A.D. 1685–1710; A.D. 1717–1732; **A.D. 1807–1890**; A.D. 1909–1928
T2-C8*	−23.8	111±35	C	A.D. 1691–1729; **A.D. 1811–1891**; A.D. 1908–1921
T2-C9*	−24.6	707±36	C	**A.D. 1218–1264**

AMS measurements were made at Van de Graff Laboratory of Utrecht (*) and at LMC14 Saclay in the frame of Artemis INSUE project. Ages were calibrated using Calib Rev 5.0 [19] and calibration curve intcal04.14c [20]. Calibrated ages exclude ranges with probability <2%, and bold ages represent the most likely intervals.

an inherited charcoal of Late Middle Ages (Fig. 7). Then, unit C should be younger than AD 1696; the oldest calendar possible age of the youngest modern samples (T2-C1, Table 1). The sample found in trench 1 comes from the base of the pedogenetized colluviums U3 and yielded a Lowermost Holocene age (≈11 000 BC), consistent with the emplacement of the previous units, U1 and U2, during the last glacial stage. Although we lack dating information for several units, the available time constraints suggest the following evolution of the faulted landscape.

Prior to the onset of Holocene global warming, efficient erosion has been reshaping and smoothing the morphology of the Krupnik Fault. Footwall erosion, down to basement rocks, decreased the slopes of the facets to 30° and was coeval with the aggradation of the thickest and oldest hangingwall colluviums found in the trenches: U1 within T1 and A1–A2, possibly B, within T2. By the onset of Holocene, slope retreat slowed down meanwhile vegetation and associated colluviated soils developed: U3 in T1 and pedogenetized colluviums B in T2. This early episode of Holocene soil formation was followed by emplacement of colluviums C in T2, and possibly base of colluviums U4 in T1. This mostly occurred by the end of the Little Ice Age (i.e., A.D. 1450–1850; [16]), and was followed by the formation of the modern soil: E in Trench T2 and U5 in Trench T1. The earthquake that disrupted the colluviums and rejuvenated the slope of the facet occurred lately. It postdates the emplacement of unit C and cannot have occurred earlier than AD 1696, oldest possible date

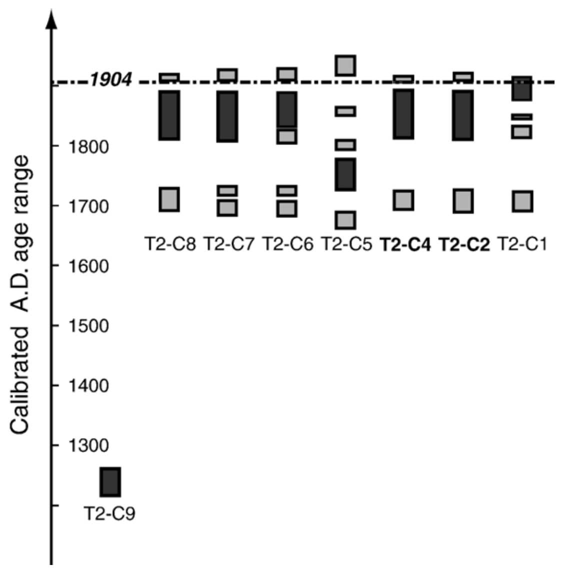

Fig. 7. Calibrated intervals for the samples collected in disrupted unit C. Dark shaded intervals are the most likely range for each sample. Samples from the fissure are indicated in bold.

obtained from the youngest modern charcoals. It could theoretically be posterior to 1953, youngest possible date obtained in unit C. This option can be turned down since the latest large event recorded in SW Bulgaria is the 1904 earthquake. Accounting that there is no historical evidence for a major earthquake in SW Bulgaria between A.D. 1696 and A.D. 1904 [7], the recent event evidenced in the trenches has to be the earthquake of 4 April 1904 (Fig. 6).

4. Summary and discussions

The paleoseismological data presented demonstrate that the Krupnik Fault hosted the 4 April 1904 Struma earthquake. Combined with detailed topographic studies, these data confirm that the recent scarp running along the mountain front is remnant of the 1904 surface break [7]. Both the scarp height and the offset of the trench units indicate about 1.5–2 m of fault slip at the surface. Assuming a usual 15 km thick brittle crust, an average fault dip of 45°, a slip of 2 m on the 20 km long Krupnik Fault yields a seismic moment Mo = 2.8 10^{19} Nm equivalent to a magnitude M_s ~6.9. This is a little less than the values of 7 to 7.2 that Ambraseys [7] has obtained from the reappraisal of the macroseismic and instrumental data, offering the possibility for a larger rupture area, a greater average slip, or both. The morphology of the Krupnik Fault makes it difficult to account for a rupture much longer than 20 km. A rupture of the neighbouring Bansko Fault is unlikely because it locates mostly outside the area of maximum intensity and has not been rejuvenated by a fresh scarp [8]. The possibility for a larger rupture-width might result either from a thicker seismogenic layer or a shallower fault dip. The slip at depth might have been also a little more than that observed at the surface allowing for a larger average slip. For instance, assuming a 20 km thick brittle crust compatible with the 40–45 km Moho depth under the Rhodope [17] and an average fault dip of 45°, an average slip of 2.5 m would have accounted for an event of Mo = 4.7 10^{19} Nm and Ms = 7.1. Alternatively, a 2.5 m slip on a ~40° dipping fault would have yielded a similar moment for a brittle crust only 15 km thick. That the results of the geomorphic study of the 1904 earthquake provide seismic moment estimates compatible with the instrumental magnitude is important. This indicates that geomorphic and paleosismic investigations do provide reliable estimates of the seismic hazard in others regions of low strain rates, whatever our knowledge of their seismicity.

The large amount of normal slip experienced during the 1904 earthquake, together with the limited depth of the trenches and the coarse stratigraphy of the units, prevented observation of former events. However, it is possible to place bounds on the age of the penultimate earthquake and on the Holocene slip-rate. The penultimate event occurred before BC 11 000 (dated charcoal from unit U3 in trench 1), and the 1904 earthquake has been the only one since then. The Krupnik Fault hence released about 2 m of seismic slip during at least the entire Holocene, in agreement with the long-term slip-rate of 0.15 mm/yr estimated since the Upper Miocene. The behavior of the Krupnik Fault bears similarities with that of the Chirpan Fault in Central Bulgaria. The latter produced the 1928 Plovdiv earthquake in central Bulgaria (Fig. 1) and has a comparable Holocene slip-rate (~0.22 mm/yr) although achieved by smaller events with ~0.5 m of seismic slip every 2.5 kyrs [18]. Moderate and infrequent earthquakes appear to typify the slow-slipping normal faults in Bulgaria. Because individual slip-rates are a few tens of mm/yr at most, further assessment of regional seismic hazard will long remain beyond the reach of the GPS techniques and requires additional geomorphic and palaeoseismological investigations. While the Krupnik and Chirpan seismogenic faults have slipped recently and are no longer of immediate concern for the seismic risk, other faults with noticeable morphology but unknown last seismic rejuvenation deserve attention. These include normal faults south of Sofia and close to the Greek border for which very little is known.

Acknowledgments

This research was carried out in the frame of a bilateral cooperation between Université Pierre et Marie Curie (UPMC) and the Bulgarian Academy of Science (BAS). Funding was provided by the SAFE European Project EVG1-2000-22005. Dating has been partly accounted for by LMC14 Saclay in the frame of INSU-CNRS ARTEMIS project. We are indebted to Elka Valova and Valo Valov for friendly technical support during fieldwork. We acknowledge constructive comments from an anonymous reviewer and helpful remarks from Claude Jaupart.

References

[1] D. Mayer-Rosa, B. Cadiot, A review of the 1356 Basel earthquake, Tectonophysics 53 (1979) 325–333.
[2] R. Bendick, R. Bilham, E. Fielding, V.K. Gaur, S.E. Hough, G. Kier, M.N. Kulkarni, S. Martin, K. Mueller, M. Mukul, The January 26, 2001 Bhuj, India earthquake, Seismol. Res. Lett. 3 (2001) , 328–335.
[3] A.C. Johnston, E.S. Schweig, The enigma of the New-Madrid earthquakes of 1811–1812, Annu. Rev. Earth Planet. Sci. 24 (1996) 339–384.
[4] M.P. Tuttle, E.S. Schweig, J.D. Sims, R.H. Lafferty, L.W. Wolf, M.L. Haynes, the earthquake potential of the New Madrid Seismic Zone, Bull. Seismol. Soc. Am. 6 (2002) 2080–2089.
[5] V. Karnik, Seismicity of the European Area. Part 1, Academy of Sciences, Praha, 1968 364 pp.
[6] E. Grigorova, K. Palieva, Macroseismic characteristics of the destructive Earthquake from 04.04.1904, Bull. Inst. Geoph., Sofia XII (1968) 109–112 (in Bulgarian, with English summary).
[7] N.N. Ambraseys, The Kresna earthquake of 1904 in Bulgaria, Annali. di Geofisica 44 (2001) 95–117.
[8] B. Meyer, R. Armijo, D. Dimitrov, Active faulting in SW Bulgaria. Possible surface rupture of the 1904 Struma earthquake, Geophys. J. Int. 148 (2002) 246–255.
[9] A. Ganas, S. Shanov, G. Drakatos, N. Dobrev, S. Sboras, C. Tsimi, G. Frangov, S. Pavlides, Active fault segmentation in southwest Bulgaria and Coulomb stress triggering of the 1904 earthquake sequence, J. Geodyn. 40 (2005) 316–333.
[10] J.A. Jackson, D.P. McKenzie, The relationship between plate motions and seismic tensors, and the rate of active deformation in the Mediterranean and Middle East, Geophys. J. Int. 93 (1988) 45–73.
[11] S. McClusky, S. Balassanian, A. Barka, C. Demir, S. Ergintav, I. Georgiev, O. Gurkan, M. Hamburger, K. Hurst, H. Kahle, K. Kastens, G. Kekelidze, R. King, V. Kotzev, O. Lenk, S. Mahmoud, A. Mishin, M. Nadariya, A. Ouzounis, D. Paradissis, Y. Peter, M. Prilepin, R. Reilinger, I. Sanli, H. Seeger, A. Tealeb, N. Toksöz, G. Veis, Global Positioning System constraints on the plate kinematics and dynamics in the eastern Mediterranean and Caucasus, J. Geophys. Res. 105 (2000) 5695–5719.
[12] H.S. Kahle, M. Cocard, Y. Peter, A. Geiger, R. Reilinger, A. Barka, G. Veis, GPS derived strain rate field within the boundary zones of the Eurasion, African, and Arabian plates, J. Geophys. Res. 105 (23) (2000) 353–370.
[13] V. Kotzev, R. Nakov, B.C. Burchfiel, R. King, R. Reilinger, GPS study of active tectonics in Bulgaria: results from 1996 to 1998, J. Geodyn. 31 (2001) 189–200.
[14] B.C. Burchfiel, R.W. King, A. Todosov, V. Kotzev, N. Durmurdzanov, T. Serafimovski, B. Nurce, GPS results for Macedonia and its importance for the tectonics of the Southern Balkan extensional regime, Tectonophysics 413 (2006) 239–248.
[15] V. Kotzev, R. Nakov, Tz. Georgiev, B.C. Burchfiel, R.W. King, Crustal motion and strain accumulation in western Bulgaria, Tectonophysics 413 (2006) 127–145.
[16] R.D. Tkachuck, The Little Ice Age, Origins 2 (1983) 51–65.
[17] R.M. Foose, F. Manheim, Geology of Bulgaria: a Review, Am. Assoc. Pet. Geol. Bull. 59 (2) (1975) 303–335.
[18] K. Vanneste, A. Radulov, P. De Martini, G. Nikolov, T. Petermans, K. Verbeeck, T. Camelbeeck, D. Pantosti, D. Dimitrov, S. Shanov, Paleoseismologic investigation of the fault rupture of the 14 April 1928 Chirpan earthquake (M 6.8), southern Bulgaria, J. Geophys. Res. 111 (2006) B01303, doi:10.1029/2005JB003814.
[19] M. Stuiver, P.J. Reimer, Extended 14C database and revised CALIB radiocarbon calibration program, Radiocarbon 35 (1993) 215–230.
[20] P.J. Reimer, M.G.L. Baillie, E. Bard, A. Bayliss, J.W. Beck, C. Bertrand, P.G. Blackwell, C.E. Buck, G. Burr, K.B. Cutler, P.E. Damon, R.L. Edwards, R.G. Fairbanks, M. Friedrich, T.P. Guilderson, K.A. Hughen, B. Kromer, F.G. McCormac, S. Manning, C. Bronk Ramsey, R.W. Reimer, S. Remmele, J.R. Southon, M. Stuiver, S. Talamo, F.W. Taylor, J. van der Plicht, C.E. Weyhenmeyer, Radiocarbon 46 (2004) 1029–1058.